ACS APPLIED ELECTRONIC MATERIALS

pubs.acs.org/acsaelm Article

High-Performance and Ultralow-Noise Two-Dimensional Heterostructure Field-Effect Transistors with One-Dimensional Electrical Contacts

Aroop K. Behera, Charles Thomas Harris, Douglas V. Pete, Collin J. Delker, Per Erik Vullum, Marta B. Muniz, Ozhan Koybasi, Takashi Taniguchi, Kenji Watanabe, Branson D. Belle, and Suprem R. Das*

Cite This: https://doi.org/10.1021/acsaelm.1c00595 Read Online

ACCESS | Metrics & More | Article Recommendations | Supporting Information

ABSTRACT: Two-dimensional heterostructure field-effect transistors (2D-HFETs) with one-dimensional electrical contacts to atomically thin channels have recently shown great device performance, such as reduced contact resistance, leading to ballistic transport and enhanced carrier mobility. While a number of low-frequency noise studies exists on bare graphene devices supported on silicon dioxide gate insulators with surface contacts, such studies in heterostructure devices comprising epitaxial graphene on hexagonal boron nitride (hBN) with edge contacts are extremely limited. In this article, we present a systematic, temperature-dependent study of electrical transport and low-frequency noise in edge-contacted high-mobility HFET with a single atomic-layer graphene channel encapsulated by hBN and demonstrate ultralow noise with a Hooge parameter of $\approx 10^{-5}$. By combining measurements and modeling based on underlying microscopic scattering mechanisms caused by charge carriers and phonons, we directly correlate the high-performance, temperature-dependent transport behavior of this device with the noise characteristics. Our study provides a pathway towards engineering low-noise graphene-based high-performance 2D-FETs with one-dimensional edge contacts for applications such as digital electronics and chemical/biological sensing.

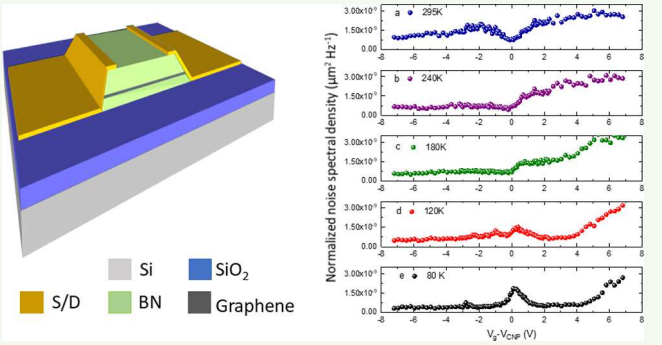

KEYWORDS: *hBN−graphene−hBN heterostructure FET, edge-contacted FET, remote interfacial phonon, 1/f noise, high-mobility FET*

INTRODUCTION

Owing to its unique electronic properties such as linear dispersion and zero band gap, graphene has been a subject of immense study over the past one and half decades.[1−5] Graphene's exceptional physical attributes, namely its high carrier mobility and high thermal conductivity, make it a very attractive material system for electronic devices such as field-effect transistors (FETs) and sensors. Because the performance of FETs and other electronic devices is limited ultimately by carrier scattering, understanding the mechanisms behind scattering is essential for improving device performance and reliability. While charge carriers in a single-layer graphene (SLG) channel have been always prone to scattering from oxide dielectrics such as SiO_2, graphene on hexagonal boron−nitride forms an epitaxial interface and has shown outstanding transport properties such as observation of high mobilities.[6]

Low-frequency electronic noise, in combination with transport measurements, can be used for fundamental studies in identifying scattering mechanisms. They are also being increasingly used as a device metric for new materials and new designs in emerging electronic devices. In semiconductor devices, low-frequency noise (LFN), demonstrating mobility fluctuations, often follows Hooge's empirical formula $\alpha_H = (S_I/I^2)(Nf^\gamma)$, where S_I is the noise power spectral density, I is the drain current, N is the total number of charge carriers that participate in the transport, f is the frequency, γ is an exponent with $\gamma \approx 1$ for most of the FETs, and α_H is the Hooge's parameter.[7] Several research groups have reported LFN $(1/f)$ in single and multilayer graphene-channel FETs,[8−14] with the most common noise studies performed on FETs fabricated on SiO_2.[8,10] Research shows that for pristine high-quality graphene (such as those from highly oriented pyrolytic graphite), which has essentially the absence of structural

Received: July 5, 2021

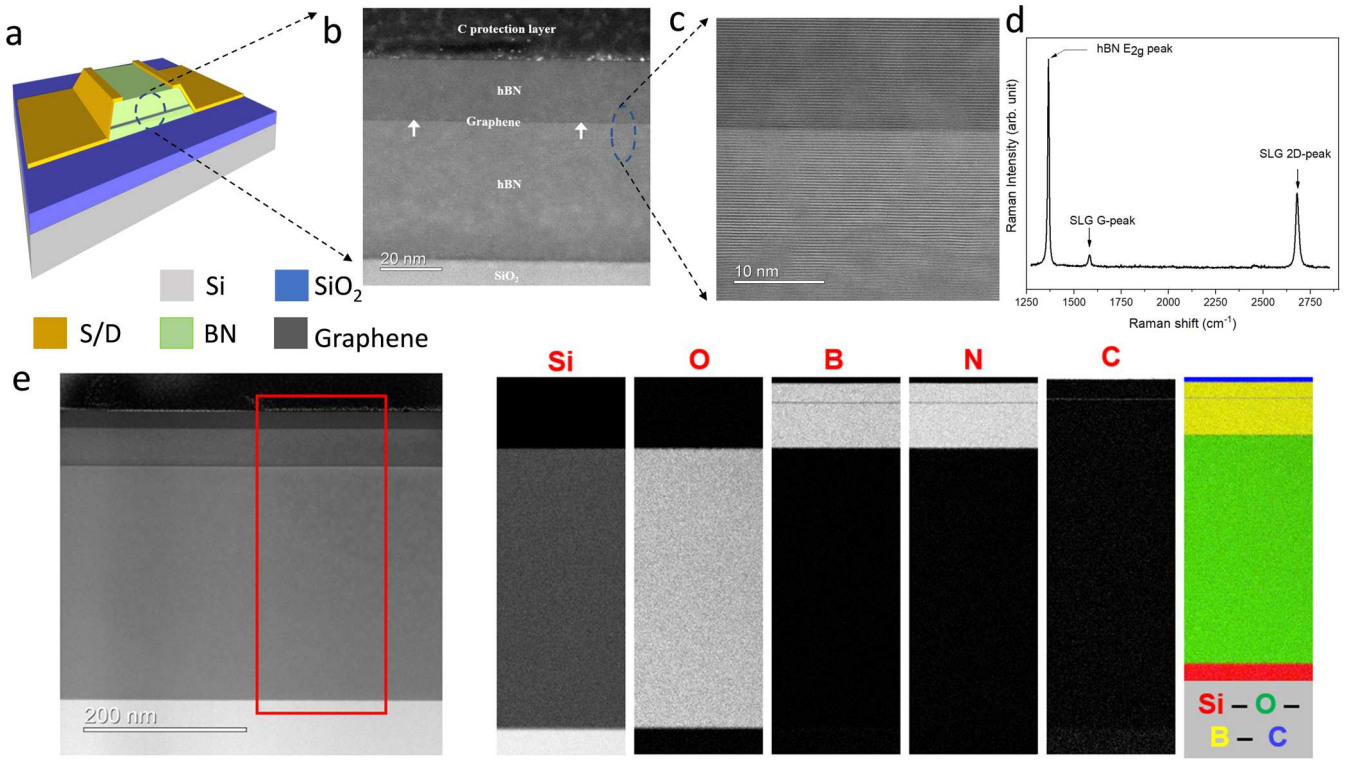

Figure 1. (a) Schematic image of the edge-contacted hBN/G/hBN 2D-HFET, (b,c) low-resolution and high-resolution cross-sectional LAADF STEM image of the channel, respectively. (d) Raman spectrum of the hBN−graphene−hBN heterostructure and (e) element mapping by EELS from inside of the red frame on the STEM image.

defects, the carriers in the channel generally experience scattering from extrinsic sources such as charge impurities from the substrate and surface,[15−17] phonons from within the graphene,[18−20] and remote interfacial phonons from the substrate.[18] Suspended graphene devices with room-temperature mobilities approaching 2×10^5 cm^2/V s[14,18] are appealing for electronics but are challenging to fabricate and structurally fragile. High-mobility graphene FETs fabricated on and encapsulated by hexagonal boron nitride (hBN) have exhibited mobility values of 1.4×10^5 cm^2/V s at room temperature[6] and have become a topic of high research interest. Further studies on FETs with graphene on hBN (hBN/graphene) and encapsulated graphene (hBN/graphene/hBN) heterostructure show that the noise in these devices is substantially reduced compared to devices fabricated on SiO_2 dielectrics.[21,22] A recent study on engineered graphene FET devices with edge contacts and hBN encapsulation and with introduction of an MoS_2 active screening layer has shown ultralow noise at room temperature.[23] High-quality electrical contacts to 2D-FET channels have become critical for the device performance, leading to many potential applications, among which 1D edge contacts to 2D heterostructure along the edges of the stack have shown lower contact resistance and superior transport properties including ballistic transport at low temperatures.[24] However, the microscopic origin of LFN and its correlation to electrical transport in these 1D edge-contacted 2D FETs have not been explored but has an important question to fundamentally understand. In this article, we study the impact of various scattering mechanisms on electrical transport and LFN in these novel edge-contacted devices.

DEVICE FABRICATION AND EXPERIMENT

hBN/graphene/hBN (hBN-G-hBN) devices (length: 6 μm, width: 2 μm) were fabricated using a dry transfer method with viscoelastic stamping.[25] Our stack consists of a SLG on a ≈50 nm hBN and is encapsulated by ≈20 nm hBN (Figure 1). One-dimensional (1D) contacts[24] were created using electron beam lithography and reactive ion etching, with 5 nm Ti and 80 nm Au being used as the edge-contacted S/D materials. Prior to any measurements, the devices were annealed at 300 °C in a H_2/Ar environment for 3 h. Figure 1a shows the schematic diagram of the edge-contacted two-dimensional heterostructure field-effect transistor (2D-HFET) device (see Supporting Information S1 for detailed transfer and fabrication). To confirm the material stack in our hBN-G-hBN 2D-HFET channel, we analyzed the structure using cross-sectional transmission electron microscopy (TEM) and scanning TEM (STEM) combined with electron energy loss spectroscopy (EELS). Figure 1b,c show cross-sectional low-angle annular dark field STEM (LAADF STEM) micrographs of the device stack and the high-resolution interface of hBN and graphene, respectively. Figure 1d shows the Raman spectrum of the hBN/graphene/hBN heterostructure using a 532 nm excitation source. The spectrum clearly shows the presence of SLG Raman peaks ($I_{2D} \gg I_G$) as well as the hBN primary peak. Figure 1e shows the elemental composition revealed by EELS. Clearly, our device shows a heterostructure with atomically aligned and flat layers with a stoichiometrically pure channel material.

Next, we performed temperature-dependent transport and noise measurements over the range of 80−300 K. Two Keithley 2400 source measurement units (SMUs) provided the gate and source-to-drain voltage biases. These SMUs were

https://doi.org/10.1021/acsaelm.1c00595
ACS Appl. Electron. Mater. XXXX, XXX, XXX−XXX

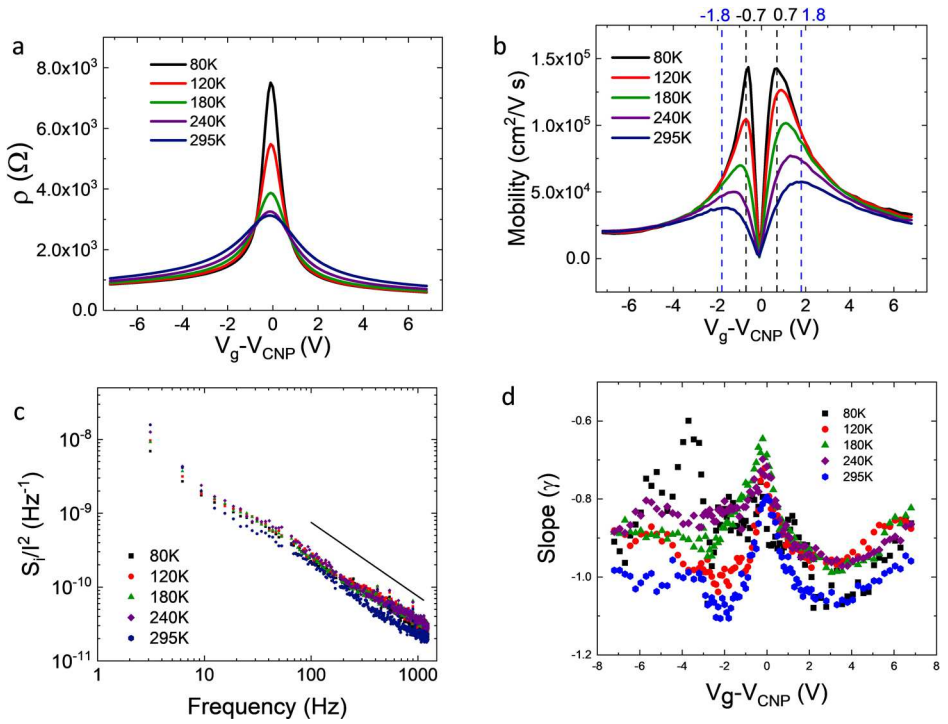

Figure 2. (a) Resistivity vs overdrive voltage characteristics of the hBN-G-hBN device, (b) extracted mobility vs gate voltage. The dotted lines depict the boundaries for the residual charge region in the device. (c) Measured normalized current noise spectrum as a function of frequency for different temperatures at a constant gate voltage ($V_g - V_{CNP}$) of 6.8 V. A solid line with slope = −1 is drawn for visual representation. (d) Obtained values of the slope γ for various temperatures at different $V_g - V_{CNP}$ values.

accompanied by low-pass RC filters to remove any spurious noise potentially originating from the SMUs and/or external voltage sources. The source-to-drain current was fed into a transimpedance amplifier (DL Instruments 1211), and the output from the amplifier was delivered to an HP-34401 digital multimeter and an HP-3588A spectrum analyzer to obtain current values and the corresponding power spectral density. All electrical measurements were carried out in a three-terminal device configuration with the heavily doped Si substrate used as a back gate.

RESULTS AND DISCUSSION

Figure 2a shows the measured resistivity (ρ) as a function of the applied gate voltage with an offset from the charge neutrality point (CNP) for various temperatures (see Supporting Information S2 for corresponding I_{ds} vs $V_g - V_{CNP}$). The resistivity peaks at the CNP reduces as the gate voltage increases on both p-side and n-side, with the highest peak occurring at the lowest temperature. The temperature-dependent resistivity of our hBN-G-hBN device exhibits behavior qualitatively similar to that reported for suspended graphene samples.[26] Approximately |1 V| beyond the CNP, the sample displays a metallic behavior where ρ increases with temperature. In such a highly carrier density-modulated system, it is important to define the region of interest for $1/f$ noise study. Unlike in a traditional FET, where a device is typically probed in its ON state, here, we considered a region with homogeneous 2D charge carrier density. This region is achieved beyond a particular overdrive voltage (i.e., $|V_g - V_{CNP}| \geq V_{CNR}$, where V_{CNR} defines a charge residual region[27]), where the resistivity increases with increase in temperature (Figure 2a). This metallic-type behavior still provides high carrier mobility even though it arises due to various scattering mechanisms as will be shown later. This is particularly true for high-quality graphene due to its exceptional electronic properties.

The field-effect mobility (μ_{FE}) was extracted for the channel using the expression

$$\mu_{FE} = \frac{g_m}{C_{ox} \times V_{ds}} \frac{L}{W} \quad (1)$$

where g_m is the transconductance, V_{ds} is the drain-source voltage (5.5 mV for these measurements), L is the channel length, W is the channel width, and C_{ox} is the oxide capacitance per unit area. g_m is calculated by (dI_{ds}/dV_g), where I_{ds} is the drain-source current and V_g is the gate voltage. C_{ox} is given by (ϵ_{ox}/d_{ox}), where ϵ_{ox} is the dielectric constant of the gate dielectric and d_{ox} is the gate-dielectric thickness. Note that in our back-gated device, a thick layer of hBN exists between the SiO_2 and the channel. Estimates show that by treating the SiO_2 and the hBN as two series capacitors, the equivalent capacitance is set by the SiO_2.

For SiO_2, ϵ_{ox} is 3×10^{-11} F/m and with d_{ox} = 300 nm, C_{ox} = 1×10^{-4} F/m^2. Figure 2b shows the carrier mobility for applied gate voltages at different temperatures. The onset of maximum carrier mobilities is indeed seen at the overdrive voltage corresponding to the crossover from the metallic to nonmetallic state of the channel. As the gate voltage increases beyond the charge residual region, the carrier scattering in the channel gradually increases, leading to a reduced extrinsic mobility and saturated channel conductivity (equivalent to the ON state of a conventional FET device). A peak mobility value of ≈60,000 cm^2/V s for electrons and ≈35,000 cm^2/V s for holes was obtained at room temperature (295 K) with a significant increase to ≈145,000 cm^2/V s at 80 K for electrons

https://doi.org/10.1021/acsaelm.1c00595
ACS Appl. Electron. Mater. XXXX, XXX, XXX−XXX

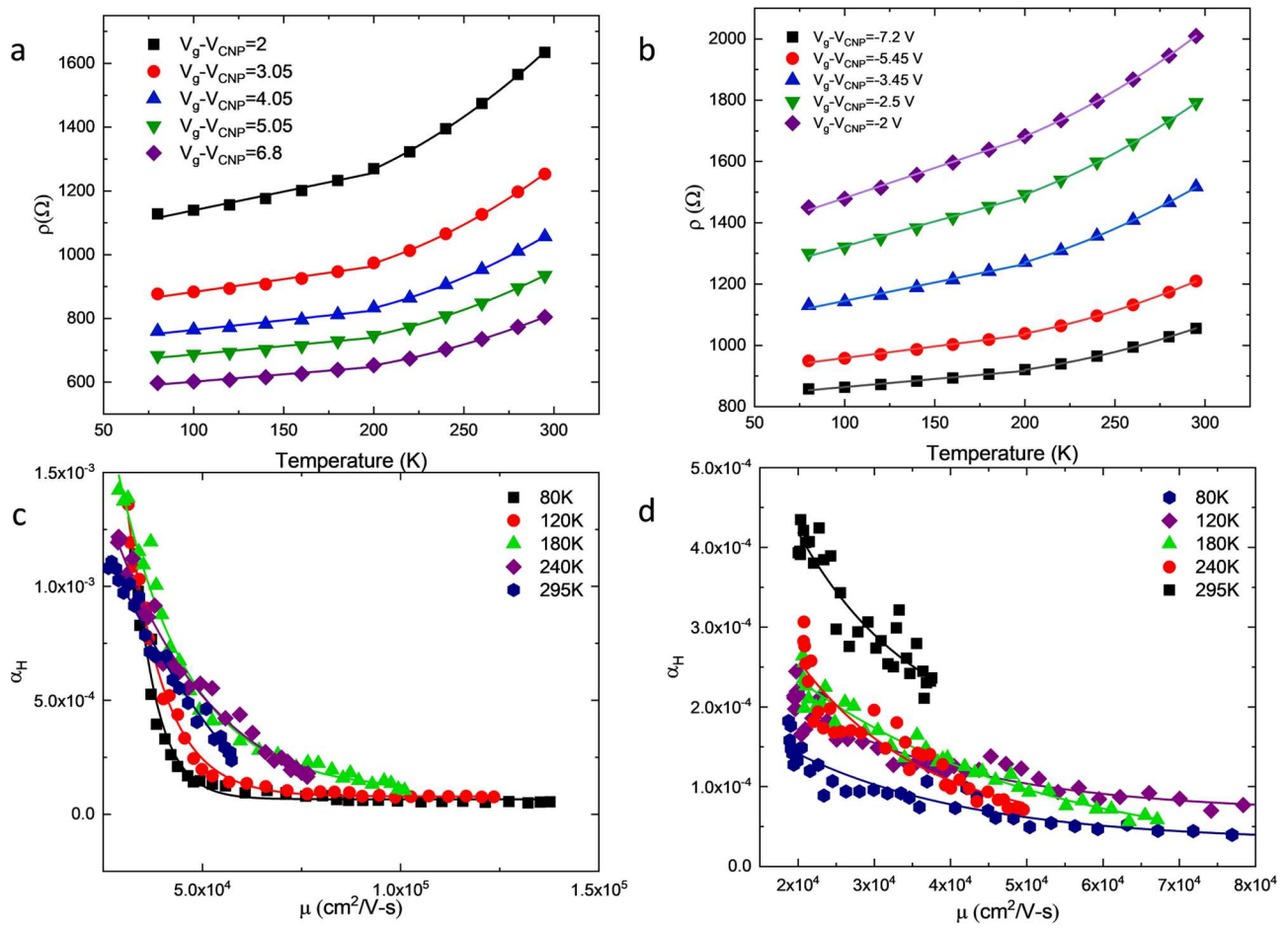

Figure 3. Resistivity as a function of temperature for electrons (a) and for holes (b). The solid lines depict the fitting in accordance with the calculated ρ. Hooge parameter α_H vs μ for electrons (c) and for holes (d). The solid lines show the exponential fitting described in the text.

and holes (Figure 2b). Such high mobility values of carriers show the outstanding screening effects by hBN.

Next, the noise measurements were taken for a series of gate voltages. Figure 2c shows the normalized current noise spectrum density versus frequency over the measured temperature range for a specific gate voltage of $(V_g - V_{CNP})$ of 6.8 V. The device exhibits $1/f$ noise behavior (the solid black line for reference). Figure 2d shows the frequency exponent at 100 Hz extracted at different temperatures and at various gate voltage values. The value of γ between 0.8 and 1.1 beyond the residual charge region indicates the validity of LFN in the edge-contacted 2D-HFET devices, further allowing us to delve into its origin. Prior reports on noise in graphene FETs involving graphene−hBN and hBN-G-hBN channels attribute an order of magnitude reduction in noise due to the screening of charge carriers by hBN from the trap states and surface defects present in SiO_2.[21,22] However, the scattering and noise mechanisms in high-performance hBN-G-hBN 2D-HFETs are still not well studied. To understand the LFN and its microscopic origin, we first analyzed the temperature-dependent resistivity data in the ON regime, that is, at $|V_g - V_{CNP}| \geq V_{CNR}$, discussed earlier.

Figure 3a,b show the temperature-dependent resistivity for electrons and holes, respectively, at selected gate voltages. Such temperature-dependent variations of resistivity in edge-contacted hBN-G-hBN 2D-HFETs arise from the scattering mechanisms that affect the mobility (and resistivity) of the FET channel.[24] An effective scattering mechanism consisting of short range and long range scatterers,[15] longitudinal acoustic (LA) phonons, and remote interfacial phonons (RIPs) could be responsible for device transport. The device resistivity based on these mechanisms can be modeled as $\rho = \rho_\circ + \rho_A + \rho_B$, where $\rho_\circ$ is a V_g dependent term, ρ_A is the resistivity contribution due to scattering of carriers from LA phonons, and ρ_B is the resistivity contribution due to scattering of carriers from RIPs. ρ_A is given by[18,19,26]

$$\rho_A = \frac{\pi D^2 k_B T}{4e^2 \hbar \rho_m v_f^2 v_{ph}^2} \tag{2}$$

where D is the acoustic deformation potential, $\rho_m = 7.6 \times 10^{-8}$ g/cm^3 is the graphene mass density, $v_{ph} = 2 \times 10^4$ m/s is the longitudinal phonon velocity, $v_f = 1 \times 10^6$ m/s is the Fermi velocity, and $\hbar$ and k_B are the reduced Planck constant and Boltzmann's constant, respectively. For ρ_B, we use the expression

$$\rho_B = \frac{B}{\sinh[\hbar\omega_o/(k_B T)]} \tag{3}$$

which has been used for hBN substrates,[28] where ω_o is the surface phonon frequency of hBN and $\hbar\omega_o$ = 101.6 meV. Using the above expressions for ρ_B (which is present above 200 K[18,28,29]) and $\rho_\circ$ and ρ_A (in the entire temperature range), ρ was obtained as a parameterized function of $V_g - V_{CNP}$. As observed in Figure 3a,b, the total resistivity (ρ) shows a linear

https://doi.org/10.1021/acsaelm.1c00595
ACS Appl. Electron. Mater. XXXX, XXX, XXX−XXX

dependence on temperature from 80 to 200 K. This linear dependence is reminiscent from the resistivity contributions from $\rho_\circ$ and LA scattering only (see Figure S5, red scatter). The nonlinearity in total resistivity (ρ) vs $V_g - V_{CNP}$, as shown in Figure 3a,b, on the other hand, is reminiscent from the collective contributions from $\rho_\circ$, LA scattering, and RIP scattering (see Figure S5, black scatter). The V_g dependence of $\rho_\circ$ (temperature-independent) has been stated previously and is attributed to the residual resistivity arising from short-range and long-range scattering at low temperature[18] (Supporting Information S3). Note that the acoustic deformation potential involved in ρ_A has been shown in Supporting Information S4.

In order to understand how the above scattering events will lead to the noise in these 2D-HFETs with 1D edge-contacts, we performed LFN measurements by monitoring the normalized current noise spectral density from 2 Hz to 1.25 kHz (Figure 2c). As shown in Figure 2d, with γ between 0.8 and 1.1 for most of the temperature values and for $|V_g - V_{CNP}| \geq V_{CNR}$, one expects that $(S_I/I^2) \propto f^{-\gamma}$ and $(S_I/I^2) \propto N^{-1}$, where N is the average charge carrier number in the channel, leading to Hooge's relation $S_I/I^2 = \alpha_H/(N \times f')$. The average noise amplitude over all the measured frequencies can be written as

$$A = \frac{\alpha_H}{N} = \frac{1}{N'}\sum_{i=1}^{N'} f_i^{\gamma}(S_I/I^2)_i \tag{4}$$

In this equation, both A and α_H are dimensionless quantities that are characteristics of the electronic noise in the device.

Figure 3c,d shows the obtained α_H as a function of μ_{FE} at f = 100 Hz for various temperatures. In order to understand how the transport signatures relate to the charge carrier scattering and noise, we analyzed the Hooge parameter versus mobility of electrons and holes. Since, α_H is directly related to noise amplitude A (eq 4), correlation of α_H and μ should provide information on A as it relates to μ and thus the scattering events we discussed previously. We obtained α_H values between 2.41×10^{-5} and 5.67×10^{-4} for holes and between 5×10^{-5} and 1.4×10^{-3} for electrons. These represent very small values of α_H in graphene devices that are promising for practical applications. The Hooge parameter could be fitted to mobility following $\alpha_H = C_1 + C_2\, e^{-C_3\mu}$, where C_1, C_2, and C_3 are fit parameters. The corresponding fitting is shown in Figure 3c,d. The power law dependence of the Hooge parameter on mobility can also be visualized as a linear behavior in a log−log plot (Supporting Information Figure S8). In addition to the mobility dependence, the Hooge parameter will also be influenced by the density of trap states (DOTS) with both the mobility and DOTS dependent on temperature. Since our analysis is at $|V_g - V_{CNP}| > V_{CNR}$, where mobility and trap states are dependent on temperature, the Hooge parameter can be written as

$$\alpha_H = f(\mu(V_g, T), D_{trap}(\epsilon, T)) \tag{5}$$

where $D_{trap}(\epsilon,T)$ is the distribution of trap states in energy and temperature.[30] The average noise amplitude then becomes

$$A = \frac{1}{N} \times f(\mu(V_g, T), D_{trap}(\epsilon, T)) \tag{6}$$

This functional dependence of α_H on V_g and T is deeply connected to the crystal lattice, interfaces between atomic layers, crystal defects, as well as the interface and trap states, and thus, it makes the noise amplitude fundamentally complex to characterize. However, under certain conditions such as at very high V_g where μ does not have a temperature dependence, α_H can be decoupled into temperature-independent and temperature-dependent terms. In a more general case such as ours, at the onset of the ON state of the device ($|V_g - V_{CNP}| \geq V_{CNR}$), we have

$$\mu_{eff} = \left[\frac{1}{\mu_{SRS}} + \frac{1}{\mu_{LRS}} + \frac{1}{\mu_{LA}} + \frac{1}{\mu_{RIP}}\right]^{-1} \tag{7}$$

where μ_{SRS}, μ_{LRS}, μ_{LA}, and μ_{RIP} are individual mobility contributions for short-range scattering, long-range scattering, LA phonon modes, and RIP modes, respectively. Therefore, in our case

$$A = \frac{1}{N} \times f(\mu_{eff}(V_g, T), D_{trap}(\epsilon, T)) \tag{8}$$

The shape of A vs V_g depends on the interplay between the four abovementioned scattering mechanisms. Figure 4a−e show the measured values of normalized current noise spectrum versus $V_g - V_{CNP}$ for selected temperature values. Using the parametric values of C_1, C_2, and C_3 obtained from Figure 3c,d, mobility (from fitting of $\rho(T)$), and the number of charge carriers in our device, we obtained the expected A versus $V_g - V_{CNP}$ behavior (the solid lines in Figure 4a−e). To compare our results with the ones reported in the literature, we also present noise spectral density normalized by the device area shown in Supporting Information S6.[31−33] Our results show an order of magnitude lower normalized current noise density. Our edge-contacted device presented here demonstrates a lower level of noise due to lower contact resistance as

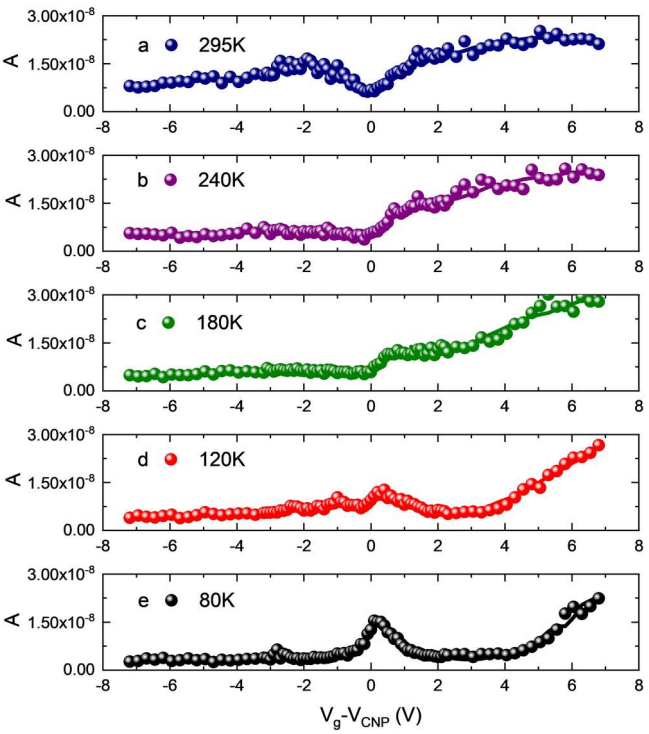

Figure 4. (a−e) Gate voltage dependence of normalized current noise amplitude at selected temperatures. The solid lines show the expected A versus $V_g - V_{CNP}$ obtained from the parametric values of C_1, C_2, and C_3 from Figure 3c,d, mobility, and number of charge carriers in the device.

https://doi.org/10.1021/acsaelm.1c00595
ACS Appl. Electron. Mater. XXXX, XXX, XXX−XXX

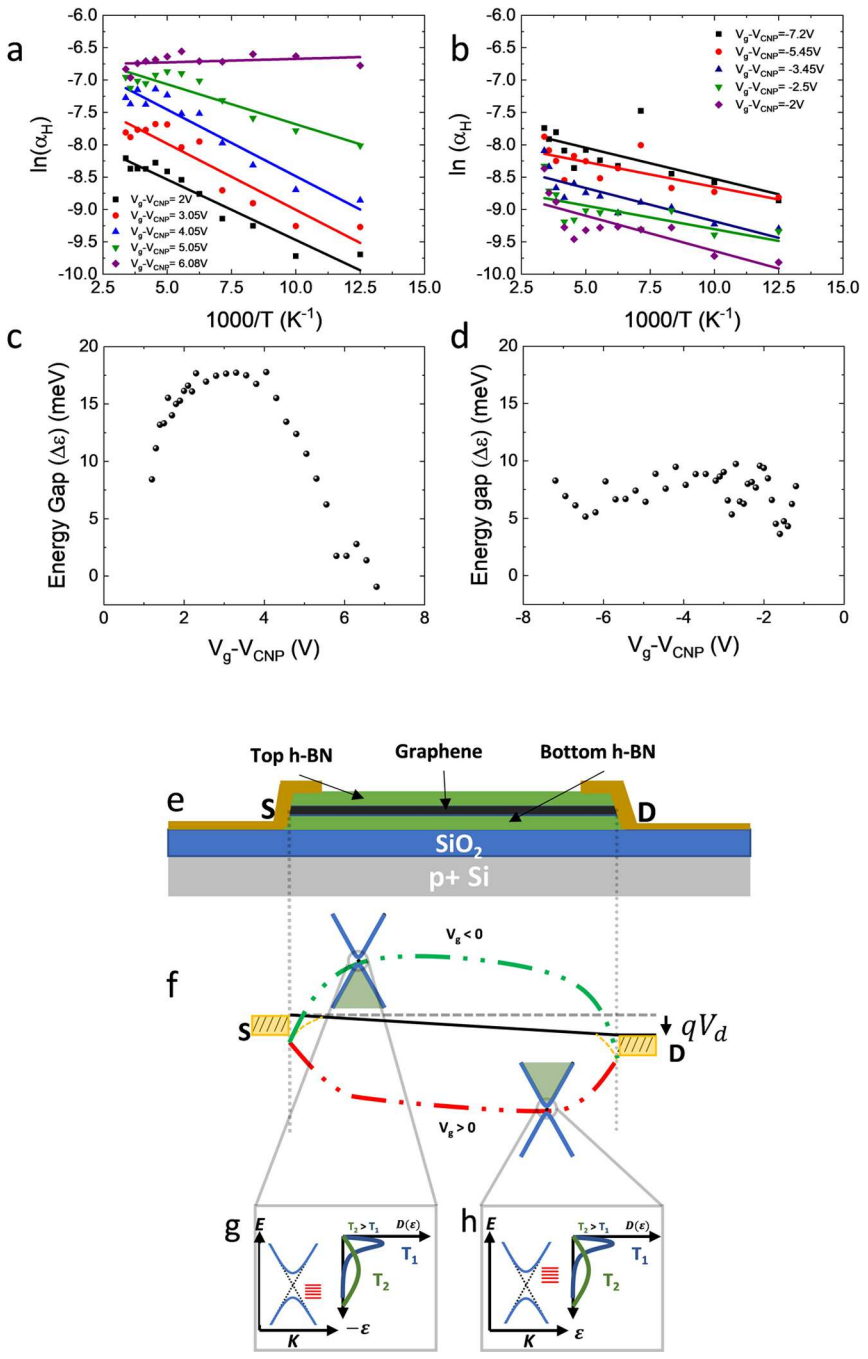

Figure 5. $\ln(\alpha_H)$ vs $1000/T$ for electron (a) and holes (b) in the device measured at various $V_g - V_{CNP}$, showing the activation energies of the distributed trap states. (c,d) Show the trap-state energies as a function of $V_g - V_{CNP}$ for electrons and holes, respectively, measured from the conduction band edge and valence band edge. (e) Schematic diagram of the 2D heterostructure FET with 1D metal contact. (f) Band diagram of the operating device for positive and negative gate bias with small drain-source bias. (g,h) Distribution of trap states and their density of states for holes and electrons, respectively.

compared to a surface-contacted device, leading to a higher transfer length and a uniform current injection from 1D contacts to the channel without current crowding.[34,35]

The temperature-dependent noise amplitude A (see eqs 4 and 8), for both electrons and holes, has been shown systematically from room temperatures 295 K down to 80 K. The carriers experience resistances from three types of scattering, that is, short- and long-range scattering (for convenience, we group these two types into one, called residual scattering), LA phonon scattering, and RIP scattering. We consider each scattering mechanism to be a different source of noise in the graphene channel. For simplicity, we consider different temperature ranges and relative strengths of these scatterers therein to decouple the contribution of each scattering mechanism toward the net noise amplitude. Below 200 K, the residual scattering and LA scattering contribute, whereas above 200 K, all of them contribute with LA contribution being much smaller as compared to the RIP contribution (see Supporting Information S3 and S5). Note that the residual scattering is independent of temperature and

https://doi.org/10.1021/acsaelm.1c00595
ACS Appl. Electron. Mater. XXXX, XXX, XXX−XXX

is responsible for the highest noise resistance among the three at any given temperature. A two-scatterer problem (both in T < 200 K and in T > 200 K) with two separate noise sources with resistance R_1 and R_2 will give the total noise amplitude in the HFET as follows

$$A = \frac{S_I \times f}{I^2} = \frac{S_{R_{tot}} \times f}{R_{tot}} = \frac{S_{R_1} + S_{R_2}}{(R_1 + R_2)^2} \quad (9)$$

where S_{Rtot} is the total noise spectral density, S_{R1} and S_{R2} are the respective noise spectral density from two scatterers, R_{tot} is the total resistance, and R_1 and R_2 are individual resistances.

In the temperature regime between 80 and 200 K, the rate of change of noise amplitude A with temperature T can be approximated by (see Supporting Information S7)

$$\frac{dA}{dT} = \frac{f}{\rho_\circ^2}\frac{dS_{\rho_{LA}}}{dT} \quad (10)$$

where f = 100 Hz, $\rho_\circ$ is the residual resistance at low temperature (T-independent), and $S_{\rho LA}$ is the noise spectral density from LA phonon contributions only. Similarly, in the temperature regime between 200 and 295 K, the rate of change of noise amplitude is given by (Supporting Information S7)

$$\frac{dA}{dT} = \frac{f}{\rho_\circ^2 T^2}\frac{dS_{\rho_{RIP}}}{dT} \quad (11)$$

As T decreases from RT to 200 K for electrons (see Figure 4), the factor $(f/\rho_\circ^2 T^2)$ increases rapidly (T^2 decreases rapidly). On the other hand, the factor $dS_{\rho RIP}/dT$ decreases rapidly (Supporting Information S5). Therefore, the noise amplitude, A, remains unchanged largely from 295 to 200 K for electrons (Figure 4). A decrease in the magnitude of A in the same temperature range for holes, on the other hand, is attributed to their higher residual resistivity ($\rho_\circ$) compared to the electrons (Supporting Information S3), leading to a smaller increasing factor $(f/\rho_\circ^2 T^2)$ (eq 11). In the temperature regime between 200 and 80 K, where the LA scattering dominates over RIP scattering, as the temperature decreases, $(f/\rho_\circ^2)$ remains constant and $(dS_{\rho LA}/dT)$ decreases (eq 10), leading to a decrease in A. An absence of any visible decrease in A between 200 and 80 K might be due to the higher $\rho_\circ$ value in the hole branch (Supporting Information S3). The temperature dependence nature of these competing scattering mechanisms apparently turns the "V-shaped" noise amplitude at room temperature gradually to a "Λ-shaped" one at low temperature. At high overdrive voltages, the carrier concentration saturates, and hence, the resistivity.

In order to find the thermally activated trap states and their activation energies, we considered the Hooge parameter (or the noise amplitude) at large gate voltages where the mobility and the DOTS dependence on the Hooge parameter could be decoupled and one can write

$$\alpha_H = f(\mu(V_g)) \times D_{trap}(\epsilon, T) \quad (12)$$

If $\Delta\epsilon$ is the activation energy of distribution of trap states, one can rewrite Hooge the parameter in terms of temperature dependence as follows

$$\alpha_H = A\, e^{-\Delta\epsilon/k_B T} \quad (13)$$

Figure 5a,b show plots of ln α_H versus $1/T$ for various overdrive voltages (including low $(V_g - V_{CNP})$ values) for electrons and holes respectively, with various slopes corresponding to the activation energies of trap states. In Figure 5c,d, we plot the extracted activation energies versus $(V_g - V_{CNP})$ for electrons and holes, respectively. Therefore, the trap states are situated within 20 meV below the conduction band edge for electrons and within 10 meV above the valence band edge for holes. Indeed, this is reasonable, given a recent prediction of a band gap opening of ≈120 meV between the valence and conduction bands in hBN-G-hBN heterostructures.[36] Based on the above analysis, a schematic band diagram of the hBN-G-hBN 2D-HFET working device with S/D edge contacts is illustrated in Figure 5e,f. Figure 5g,h illustrate the schematic band diagram, distribution of shallow trap states within the energy gap, and the DOTS with their temperature dependence near the conduction band edge and valence band edge, respectively.

CONCLUSIONS

To summarize, we have demonstrated a systematic temperature-dependent measurement of LFN in two-dimensional hBN/SLG/hBN heterostructure FET devices with 1D metal contacts. The study was carried out by showing high-performance device quality of our FETs with mobilities of 60,000 $cm^2/V\,s$ for electrons and 35,000 $cm^2/V\,s$ for holes at room temperature and 145,000 $cm^2/V\,s$ for electrons and holes at low temperature (80 K). We have shown very low $1/f$ noise in these devices with a characteristic Hooge parameter approaching $\approx 10^{-5}$, a value recommended by the semiconductor industry for future high-performance silicon nanoelectronic devices. By systematically studying the temperature-dependent transport and noise characteristics in these devices, we have developed a noise model on mobility fluctuation by fundamentally correlating it with the underlying microscopic scattering mechanisms such as short-range scattering, long-range scattering, LA scattering, and remote interfacial scattering. We have used the temperature-dependent noise measurements to extract the energy of shallow electron and hole trap states within 20 meV energies from respective band edges, a study that could be utilized for future noise engineering. Our study paves the way for developing strategies for further designing of high-performance and ultralow 2D-HFET devices with 1D edge contacts that could find applications in a number of domains such as digital electronics and chemical/biological sensing.

ASSOCIATED CONTENT

Supporting Information

The Supporting Information is available free of charge at https://pubs.acs.org/doi/10.1021/acsaelm.1c00595.

Device fabrication; drain-source current versus $V_g - V_{CNP}$; residual resistance extraction; deformation potential extraction; LA and RIP resistivity extraction; noise spectral density normalized by device area; derivations for the rate of change of noise amplitude A with temperature; and power law dependence of the Hooge parameter on mobility (log–log plot) (PDF)

AUTHOR INFORMATION

Corresponding Author

Suprem R. Das − *Department of Industrial and Manufacturing Systems Engineering and Department of Electrical and Computer Engineering, Kansas State*

https://doi.org/10.1021/acsaelm.1c00595
ACS Appl. Electron. Mater. XXXX, XXX, XXX−XXX

University, Manhattan, Kansas 66506, United States; orcid.org/0000-0003-0334-7600; Email: srdas@ksu.edu

Authors

Aroop K. Behera − *Department of Industrial and Manufacturing Systems Engineering, Kansas State University, Manhattan, Kansas 66506, United States*

Charles Thomas Harris − *Center for Integrated Nanotechnologies, Sandia National Laboratories, Albuquerque, New Mexico 87123, United States; Sandia National Laboratories, Albuquerque, New Mexico 87185, United States*

Douglas V. Pete − *Center for Integrated Nanotechnologies, Sandia National Laboratories, Albuquerque, New Mexico 87123, United States; Sandia National Laboratories, Albuquerque, New Mexico 87185, United States*

Collin J. Delker − *Sandia National Laboratories, Albuquerque, New Mexico 87185, United States*

Per Erik Vullum − *Department of Materials and Nanotechnology, SINTEF, Trondheim NO-7034, Norway*

Marta B. Muniz − *Department of Sustainable Energy Technology, SINTEF, Oslo 0373, Norway; Institut de Physique de la Matière Complexe, Ecole Polytechnique Fèdèrale de Lausanne (EPFL), Lausanne 1015, Switzerland*

Ozhan Koybasi − *Department of Microsystems and Nanotechnology, SINTEF DIGITAL, Oslo 0373, Norway*

Takashi Taniguchi − *International Center for Materials Nanoarchitectonics, National Institute for Materials Science, Tsukuba 305-0044, Japan;* orcid.org/0000-0002-1467-3105

Kenji Watanabe − *Research Center for Functional Materials, National Institute for Materials Science, Tsukuba 305-0044, Japan;* orcid.org/0000-0003-3701-8119

Branson D. Belle − *Department of Sustainable Energy Technology, SINTEF, Oslo 0373, Norway;* orcid.org/0000-0002-1211-8714

Complete contact information is available at: https://pubs.acs.org/10.1021/acsaelm.1c00595

Author Contributions

S.R.D. conceived the original idea, designed, and supervised the project. A.K.B. performed the measurements and analysis, C.T.H., D.V.P., and C.J.D. helped in the measurement setup, B.D.B., O.K., M.B.M., and P.E.V. fabricated the devices and performed TEM, and T.T. and K.W. provided hBN.

Notes

The authors declare no competing financial interest.

■ ACKNOWLEDGMENTS

S.R.D. acknowledges, in part, the work performed at the Center for Integrated Nanotechnologies, an Office of Science User Facility operated for the U.S. Department of Energy (DOE) Office of Science. Sandia National Laboratories is a multimission laboratory managed and operated by the National Technology and Engineering Solutions of Sandia, LLC., a wholly owned subsidiary of Honeywell International, Inc., for the U.S. Department of Energy's National Nuclear Security Administration under contract no. DE-NA0003525. This paper describes objective technical results and analysis. Any subjective views or opinions that might be expressed in the paper do not necessarily represent the views of the U.S. Department of Energy or the United States Government. S.R.D. also acknowledges, in part, support from the U.S. National Science Foundation (NSF), grant no. NSF CBET # 1935676. B.D.B. acknowledges support by the Research Council of Norway (project nos. 250555 and 280788). The Research Council of Norway is also acknowledged for the support to the Norwegian Micro- and Nano-Fabrication Facility, NorFab, project number 245963/F50 and for support to the NORTEM infrastructure, grant 197405, TEM Gemini Center, NTNU, Norway. The authors acknowledge support from the Elemental Strategy Initiative conducted by the MEXT, Japan, grant number JPMXP0112101001, JSPS KAKENHI grant number JP20H00354, and the CREST(JPMJCR15F3), JST.

■ REFERENCES

(1) Novoselov, K. S.; Geim, A. K.; Morozov, S. V.; Jiang, D.; Katsnelson, M. I.; Grigorieva, I. V.; Dubonos, S. V.; Firsov, A. A. Two-dimensional gas of massless Dirac fermions in graphene. *Nature* **2005**, *438*, 197−200.

(2) Novoselov, K. S. Electric Field Effect in Atomically Thin Carbon Films. *Science* **2004**, *306*, 666−669.

(3) Geim, A. K.; Novoselov, K. S. The rise of graphene. *Nat. Mater.* **2007**, *6*, 183−191.

(4) Morozov, S. V.; Novoselov, K. S.; Katsnelson, M. I.; Schedin, F.; Elias, D. C.; Jaszczak, J. A.; Geim, A. K. Giant Intrinsic Carrier Mobilities in Graphene and Its Bilayer. *Phys. Rev. Lett.* **2008**, *100*, 016602.

(5) Das Sarma, S.; Adam, S.; Hwang, E. H.; Rossi, E. Electronic transport in two-dimensional graphene. *Rev. Mod. Phys.* **2011**, *83*, 407−470.

(6) Dean, C. R.; Young, A. F.; Meric, I.; Lee, C.; Wang, L.; Sorgenfrei, S.; Watanabe, K.; Taniguchi, T.; Kim, P.; Shepard, K. L.; Hone, J. Boron nitride substrates for high-quality graphene electronics. *Nat. Nanotechnol.* **2010**, *5*, 722−726.

(7) Hooge, F. N. 1/f noise is no surface effect. *Phys. Lett. A* **1969**, *29*, 139−140.

(8) Lin, Y.-M.; Avouris, P. Strong Suppression of Electrical Noise in Bilayer Graphene Nanodevices. *Nano Lett.* **2008**, *8*, 2119−2125.

(9) Golub, A.; Horovitz, B. Shot noise in graphene with long-range Coulomb interaction and local Fermi distribution. *Phys. Rev. B: Condens. Matter Mater. Phys.* **2010**, *81*, 245424.

(10) Xu, G.; Torres, C. M.; Zhang, Y.; Liu, F.; Song, E. B.; Wang, M.; Zhou, Y.; Zeng, C.; Wang, K. L. Effect of Spatial Charge Inhomogeneity on 1/f Noise Behavior in Graphene. *Nano Lett.* **2010**, *10*, 3312−3317.

(11) Pal, A. N.; Ghatak, S.; Kochat, V.; Sneha, E. S.; Sampathkumar, A.; Raghavan, S.; Ghosh, A. Microscopic Mechanism of 1/f Noise in Graphene: Role of Energy Band Dispersion. *ACS Nano* **2011**, *5*, 2075−2081.

(12) Liu, G.; Rumyantsev, S.; Shur, M. S.; Balandin, A. A. Origin of 1/f noise in graphene multilayers: Surface vs. volume. *Appl. Phys. Lett.* **2013**, *102*, 093111.

(13) Balandin, A. A. Low-frequency 1/f noise in graphene devices. *Nat. Nanotechnol.* **2013**, *8*, 549−555.

(14) Zhang, Y.; Mendez, E. E.; Du, X. Mobility-Dependent Low-Frequency Noise in Graphene Field-Effect Transistors. *ACS Nano* **2011**, *5*, 8124−8130.

(15) Adam, S.; Hwang, E. H.; Galitski, V. M.; Das Sarma, S. A self-consistent theory for graphene transport. *Proc. Natl. Acad. Sci. U.S.A.* **2007**, *104*, 18392−18397.

(16) Hwang, E. H.; Adam, S.; Sarma, S. D. Carrier Transport in Two-Dimensional Graphene Layers. *Phys. Rev. Lett.* **2007**, *98*, 186806.

(17) Chen, J.-H.; Jang, C.; Adam, S.; Fuhrer, M. S.; Williams, E. D.; Ishigami, M. Charged-impurity scattering in graphene. *Nat. Phys.* **2008**, *4*, 377−381.

(18) Chen, J.-H.; Jang, C.; Xiao, S.; Ishigami, M.; Fuhrer, M. S. Intrinsic and extrinsic performance limits of graphene devices on SiO2. *Nat. Nanotechnol.* **2008**, *3*, 206−209.
(19) Hwang, E. H.; Das Sarma, S. Acoustic phonon scattering limited carrier mobility in two-dimensional extrinsic graphene. *Phys. Rev. B: Condens. Matter Mater. Phys.* **2008**, *77*, 115449.
(20) Sarkar, S.; Amin, K. R.; Modak, R.; Singh, A.; Mukerjee, S.; Bid, A. Role of different scattering mechanisms on the temperature dependence of transport in graphene. *Sci. Rep.* **2015**, *5*, 16772.
(21) Kayyalha, M.; Chen, Y. P. Observation of reduced 1/f noise in graphene field effect transistors on boron nitride substrates. *Appl. Phys. Lett.* **2015**, *107*, 113101.
(22) Stolyarov, M. A.; Liu, G.; Rumyantsev, S. L.; Shur, M.; Balandin, A. A. Suppression of 1/f noise in near-ballistic h-BN-graphene-h-BN heterostructure field-effect transistors. *Appl. Phys. Lett.* **2015**, *107*, 023106.
(23) Kakkar, S.; Karnatak, P.; Ali Aamir, M.; Watanabe, K.; Taniguchi, T.; Ghosh, A. Optimal architecture for ultralow noise graphene transistors at room temperature. *Nanoscale* **2020**, *12*, 17762−17768.
(24) Wang, L.; Meric, I.; Huang, P. Y.; Gao, Q.; Gao, Y.; Tran, H.; Taniguchi, T.; Watanabe, K.; Campos, L. M.; Muller, D. A.; Guo, J.; Kim, P.; Hone, J.; Shepard, K. L.; Dean, C. R. One-Dimensional Electrical Contact to a Two-Dimensional Material. *Science* **2013**, *342*, 614−617.
(25) Castellanos-Gomez, A.; Buscema, M.; Molenaar, R.; Singh, V.; Janssen, L.; van der Zant, H. S. J.; Steele, G. A. Deterministic transfer of two-dimensional materials by all-dry viscoelastic stamping. *2D Mater.* **2014**, *1*, 011002.
(26) Bolotin, K. I.; Sikes, K. J.; Hone, J.; Stormer, H. L.; Kim, P. Temperature-Dependent Transport in Suspended Graphene. *Phys. Rev. Lett.* **2008**, *101*, 096802.
(27) Zhong, H.; Zhang, Z.; Xu, H.; Qiu, C.; Peng, L.-M. Comparison of mobility extraction methods based on field-effect measurements for graphene. *AIP Adv.* **2015**, *5*, 057136.
(28) Schiefele, J.; Sols, F.; Guinea, F. Temperature dependence of the conductivity of graphene on boron nitride. *Phys. Rev. B: Condens. Matter Mater. Phys.* **2012**, *85*, 195420.
(29) Mayorov, A. S.; Gorbachev, R. V.; Morozov, S. V.; Britnell, L.; Jalil, R.; Ponomarenko, L. A.; Blake, P.; Novoselov, K. S.; Watanabe, K.; Taniguchi, T.; Geim, A. K. Micrometer-Scale Ballistic Transport in Encapsulated Graphene at Room Temperature. *Nano Lett.* **2011**, *11*, 2396−2399.
(30) Dutta, P.; Dimon, P.; Horn, P. M. Energy Scales for Noise Processes in Metals. *Phys. Rev. Lett.* **1979**, *43*, 646−649.
(31) Rumyantsev, S.; Liu, G.; Stillman, W.; Shur, M.; Balandin, A. A. Electrical and noise characteristics of graphene field-effect transistors: ambient effects, noise sources and physical mechanisms. *J. Phys.: Condens. Matter* **2010**, *22*, 395302.
(32) Rumyantsev, S. L.; Jiang, C.; Samnakay, R.; Shur, M. S.; Balandin, A. A. 1/f Noise Characteristics of MoS2 Thin-Film Transistors: Comparison of Single and Multilayer Structures. *IEEE Electron Device Lett.* **2015**, *36*, 517−519.
(33) Zahid Hossain, M.; Rumyantsev, S.; Shur, M. S.; Balandin, A. A. Reduction of 1/f noise in graphene after electron-beam irradiation. *Appl. Phys. Lett.* **2013**, *102*, 153512.
(34) Nagashio, K.; Nishimura, T.; Kita, K.; Toriumi, A. Contact resistivity and current flow path at metal/graphene contact. *Appl. Phys. Lett.* **2010**, *97*, 143514.
(35) Karnatak, P.; Sai, T. P.; Goswami, S.; Ghatak, S.; Kaushal, S.; Ghosh, A. Current crowding mediated large contact noise in graphene field-effect transistors. *Nat. Commun.* **2016**, *7*, 13703.
(36) Quhe, R.; Zheng, J.; Luo, G.; Liu, Q.; Qin, R.; Zhou, J.; Yu, D.; Nagase, S.; Mei, W.-N.; Gao, Z.; Lu, J. Tunable and sizable band gap of single-layer graphene sandwiched between hexagonal boron nitride. *NPG Asia Mater.* **2012**, *4*, No. e6.

https://doi.org/10.1021/acsaelm.1c00595
ACS Appl. Electron. Mater. XXXX, XXX, XXX−XXX